Isolation of a Single Carboxyl-Carboxylate Proton Binding Site in the Pore of a Cyclic Nucleotide–gated Channel

James A. Morrill* and Roderick MacKinnon‡

From the *Program in Neuroscience, Division of Medical Sciences, Harvard Medical School, Boston, Massachusetts 02114, and ‡Howard Hughes Medical Institute, Laboratory of Molecular Neurobiology and Biophysics, Rockefeller University, New York 10021

abstract The pore of the catfish olfactory cyclic nucleotide–gated (CNG) channel contains four conserved glutamate residues, one from each subunit, that form a high-affinity binding site for extracellular divalent cations. Previous work showed that these residues form two independent and equivalent high-pK_a (~7.6) proton binding sites, giving rise to three pH-dependent conductance states, and it was suggested that the sites were formed by pairing of the glutamates into two independent carboxyl-carboxylates. To test further this physical picture, wild-type CNG subunits were coexpressed in *Xenopus* oocytes with subunits lacking the critical glutamate residue, and single channel currents through hybrid CNG channels containing one to three wild-type (WT) subunits were recorded. One of these hybrid channels had two pH-dependent conductance states whose occupancy was controlled by a single high-pK_a protonation site. Expression of dimers of concatenated CNG channel subunits confirmed that this hybrid contained two WT and two mutant subunits, supporting the idea that a single protonation site is made from two glutamates (dimer expression also implied the subunit makeup of the other hybrid channels). Thus, the proton binding sites in the WT channel occur as a result of the pairing of two glutamate residues. This conclusion places these residues in close proximity to one another in the pore and implies that at any instant in time detailed fourfold symmetry is disrupted.

key words: ion channel permeation • proton block • *Xenopus* oocyte expression • ligand-gated ion channels • patch clamp

introduction

Changes in pH at the intracellular or extracellular face of an ion channel under physiological or laboratory-defined conditions can have strong effects on gating or permeation properties. pH-dependent ion channel behavior, controlled by the binding of protons to important functional regions of the channel protein, has been observed for a wide variety of channel types, including voltage-dependent Na^+ (Zhang and Siegelbaum, 1991; Chahine et al., 1994), Ca^{2+} (Prod'hom et al., 1987; Krafte and Kass, 1988; Klockner and Isenberg, 1994; Chen et al., 1996), K^+ (Davies et al., 1992; Cuello et al., 1998; Reyes et al., 1998), glutamate receptor (Traynelis and Cull-Candy, 1991), and cyclic nucleotide–gated ion channels (Root and MacKinnon, 1994; Gordon et al., 1996).

In some cases, the effects of protons on ion permeation can provide insight into the detailed structure of the pore. One example is the promotion of subconductance states by the binding of H^+ to the pore of the cardiac L-type voltage-dependent Ca^{2+} channel. Unitary Ca^{2+} channel recordings in cardiac ventricular myocytes showed that the binding of protons to a single extracellular site having a pK_a of ~7.5 caused the channel to switch from a high-conductance state to a state with threefold lower conductance (Prod'hom et al., 1987). More recent investigations of this phenomenon using *Xenopus* oocyte expression of the cloned cardiac L-type Ca^{2+} channel have revealed that the proton-binding site is formed by an asymmetric cluster of four glutamate residues in the pore that also play a fundamental role in the high-affinity binding of permeant Ca^{2+} ions (Yang et al., 1993; Ellinor et al., 1995; Chen et al., 1996).

A similar phenomenon has been observed in the cloned catfish olfactory cyclic nucleotide-gated (CNG)[1] channel, a nonselective cation channel having homology to voltage-gated potassium channels (Goulding et al., 1992; Root and MacKinnon, 1994). Fig. 1 A shows a single-channel record collected at −80 mV with 130 mM NaCl, pH 7.6, on both sides of the membrane; the recording was made in the presence of deuterium oxide (^2H_2O) instead of H_2O to slow the transition rate between the three conductance states (see materials and methods). The amplitude histogram in Fig. 1 B, calculated from the activity of the channel shown in Fig. 1 A, shows three peaks, one for each of the conductance states (~70, ~42, and ~18 pS). In the model proposed by Root and MacKinnon (1994) to explain

Address correspondence to Dr. Roderick MacKinnon, Howard Hughes Medical Institute, Laboratory of Molecular Neurobiology and Biophysics, Rockefeller University, 1230 York Avenue, New York, NY 10021. Fax: 212-327-7289; E-mail: mackinn@rockvax.rockefeller.edu

[1]*Abbreviations used in this paper:* CNG, cyclic nucleotide–gated; E333G, Glu333Gly; WT, wild type.

this behavior, diagrammed in Fig. 1 C, the conductance states were controlled by protonation at two independent and equivalent sites of pK_a ~7.6: the high-conductance state occurred in the absence of bound H^+, the intermediate conductance state occurred when one or the other site was occupied by a proton, and the low conductance state occurred when both sites were occupied. This behavior was found to depend on the presence of a pore glutamate residue (Glu333) analogous to the glutamates in the pore of the cardiac L-type Ca^{2+} channel; mutation of Glu333 to glycine gave a proton-insensitive channel with a single conductance state. It was proposed that the four Glu333 residues in the pore might form two bi-symmetrical and independent carboxyl-carboxylate pairs, in each of which a H^+ ion may be shared equally between two carboxyl groups. Carboxyl-carboxylates are well described and can have high pK_a values (Sawyer and James, 1982).

The purpose of this study was to test the plausibility of the idea that the two protonation sites in the pore of the catfish olfactory CNG channel consist of two physically separate carboxyl-carboxylate pairs. The strategy we used was to create hybrid CNG channels containing a mixture of wild-type (WT) and Glu333Gly (E333G) subunits. If the sites are separate carboxyl-carboxylates, we reasoned, it should be possible to isolate a hybrid channel containing one, but not both, of the original protonation sites intact.

By expressing a mixture of WT and E333G subunits, we formed functionally WT channels, pure mutant channels, and four novel channel types, a result consistent with the postulated tetrameric structure of CNG channels. One of the novel channels, which we named Type B, had two pH-dependent conductance states whose occupancy was governed by protonation at a single site having a pK_a of 6.8. Expression of tandem dimer constructs enabled us to determine the number of WT and E333G subunits in all of the hybrid channels and revealed that the Type B channel contained two WT and two E333G subunits. We conclude that we were able to isolate, in the Type B hybrid channel, a single protonation site formed by two glutamate carboxyl groups with properties very similar to those in the native channel. Our results corroborate the hypothesis that the protonation sites in the native channel are structurally independent carboxyl-carboxylates.

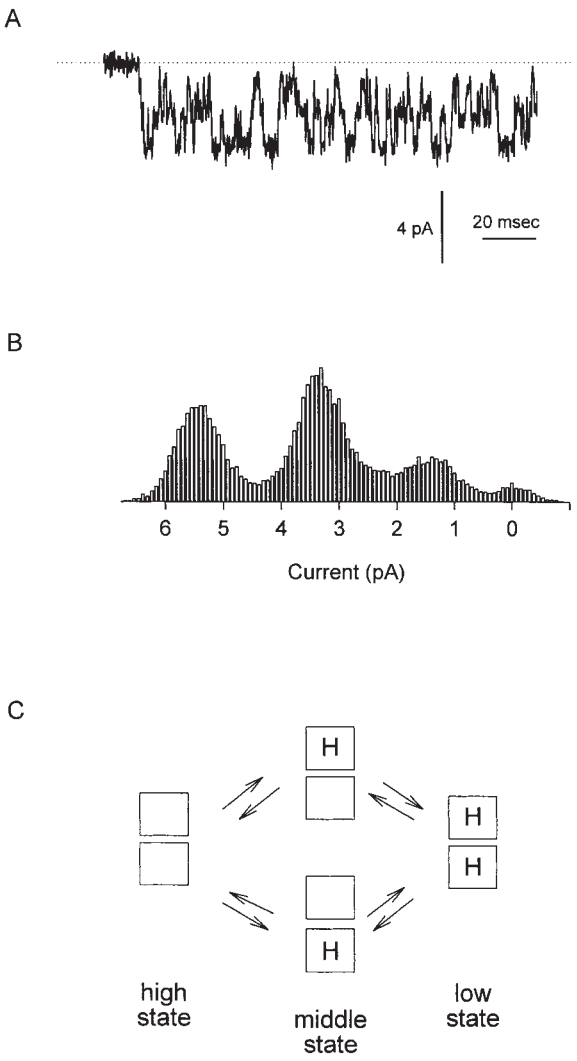

Figure 1. The wild-type catfish olfactory cyclic nucleotide–gated channel has three conductance states whose occupancy is governed by protonation at two independent and equivalent sites in the channel pore. (A) Single-channel record showing the activity of a WT catfish olfactory CNG channel. The current was recorded from an inside-out patch held at −80 mV and exposed to 130 mM NaCl, pH 7.6, on both sides of the membrane. Recording solutions were prepared using ^2H_2O to slow transitions between the three conductance levels. (B) Amplitude histogram compiled from the activity of the WT channel shown in A showing the three distinct conductance levels visited by the channel (~70, ~42, and ~18 pS). (C) Model introduced by Root and MacKinnon (1994) to explain quantitatively the behavior of the wild-type channel. In the model, four pore glutamate residues (one per subunit) combine to form two independent and equivalent protonation sites affecting ion permeation. The channel occupies the 70-pS conductance state when neither site is protonated, the 42-pS conductance state when either one of the sites is protonated, and the 18-pS conductance state when both sites are protonated.

materials and methods

Molecular Biology

The catfish olfactory CNG channel α subunit was carried in the pGEMHE plasmid (construct kindly provided by E. Goulding and S. Siegelbaum of Columbia University, New York; Goulding et al., 1992). The Glu333Gly mutation was generated in a MluI–ClaI pore cassette as previously described (Root and MacKinnon, 1994). RNA for oocyte expression was synthesized from SphI-linearized DNA using T7 RNA polymerase.

Dimer constructs were made as follows. The catfish olfactory CNG channel α subunit (WT or E333G) was subcloned into the pRSET plasmid (BamHI to HindIII) just 3′ to a 102-bp sequence

(NcoI to BamHI) encoding a 34 amino acid peptide linker. The linker, originally designed for antibody studies of the channel, contained a polyhistidine stretch followed by a T7 epitope tag and an aspartate-rich sequence. The entire linker plus channel construct (NcoI to HindIII) was excised from pRSET and inserted into a pGEMHE-CNG channel construct that had been mutated to give an NcoI site at the 3′ end of the α subunit coding sequence. The result was a construct in pGEMHE (BamHI to HindIII) consisting of two complete catfish olfactory CNG channel α subunits separated by the 102-bp linker sequence. To reduce the likelihood of contamination of dimer DNA or RNA by monomers, the following measures were taken: (a) only recA$^-$ strains of *Escherichia coli* were used to carry the dimer plasmids; (b) after the dimer ligation reaction, single colonies were picked and shown to contain a single dimer-sized species by agarose gel electrophoresis; and (c) after in vitro RNA synthesis, dimer RNA was compared side-by-side with monomer RNA on an agarose gel and shown to be free from contamination by the monomer band, which ran at a distinct position. Dimer constructs were made from the WT and E333G subunits in all possible combinations: WT:WT, WT:E333G, E333G:WT, and E333G:E333G. Dimer RNA was synthesized using T7 RNA polymerase after linearization with SphI.

Electrophysiology

Xenopus laevis oocytes were prepared and injected with CNG channel RNA as previously described (Root and MacKinnon, 1994). For experiments in which WT and E333G subunits (or WT:WT and E333G:E333G dimers) were coexpressed, a 2:1 ratio of WT:E333G RNA was injected because of the tendency of mutant subunits to express to higher levels than WT subunits. Inside-out or outside-out patches were obtained with electrodes fabricated from capillary glass (Drummond Scientific), coated with beeswax, and fire polished to a resistance of 1–5 MΩ. Single-channel currents were recorded 1–3 d after RNA injection using an Axopatch 200 amplifier (Axon Instruments). The amplifier output was filtered at 2 kHz and sampled at 10 kHz using a DAP data collection board (Microstar Laboratories). All-points amplitude histograms were constructed off-line using an analysis program written in Microsoft QuickBASIC. The bin-width of the histograms was 0.05 pA, and at least 500,000 sample points (50 s) of data were used to construct each histogram. Histograms were constructed primarily from open-channel activity, with a small amount of baseline activity included as a reference.

The internal and external solutions were made using ^2H_2O (deuterium oxide; Sigma Chemical CO.) to slow the kinetics of protonation and deprotonation events, as previously described (Root and MacKinnon, 1994). Both solutions contained (mM): 130 NaCl, 3 HEPES, and 0.5 Na_2EDTA. To activate the CNG channels, 1 mM Na-cGMP (Sigma Chemical Co.) was added to the internal solution. For experiments in which the extracellular pH was varied, outside-out patches were perfused with solutions of varying pH using a linear array of microcapillary tubes (1 μl, 64 mm special length; Drummond Scientific). Solutions were adjusted to the appropriate pH (6.0–8.5) using concentrated NaOH and HCl solutions prepared with ^2H_2O.

results

Injection of a Mixture of WT and Glu333Gly CNG Subunits Gives Rise to WT Channels, Pure Mutant Channels, and Four Hybrid CNG Channel Types

Our primary objective was to test the independence of the two protonation sites found in the WT catfish olfactory CNG channel. To do this, we asked whether it was possible to use a mixture of WT and E333G subunits to create a hybrid channel containing one but not both sites. A 2:1 mixture of WT and E333G subunit RNA was injected into *Xenopus* oocytes, and single CNG channels were recorded from inside-out patches at a holding voltage of −80 mV, with 130 mM NaCl, pH 7.6, on both sides of the membrane. The varieties of single channels found are shown in Fig. 2 A. In the first two columns, individual examples of current traces are presented alongside amplitude histograms calculated for the same channels. Pure mutant channels with a single conductance state of ∼25 pS were observed (Fig. 2 A, top), as were WT channels having the usual three conductance states of 65–70, 35–40, and 15–20 pS (Fig. 2 A, bottom). In addition, four novel types of hybrid channels were found, which we have called Types A, B, C, and D. The Type A channel had no single well-defined conductance state, spending most of its time at low (∼30 pS) conductances, but also displaying brief spikes to higher conductances (which gave rise to the long tail in the amplitude distribution). The Type B channel appeared to have two well-separated conductance states of ∼50–65 and ∼25–40 pS, with the higher conductance state favored at pH 7.6. The Type C channel appeared to jump rapidly between poorly distinguished conductance levels and visited both lower and higher conductances from its main conductance level of ∼50–60 pS, behavior that gave both high- and low-conductance tails in the amplitude histogram. The Type D channel appeared in single-channel records to show behavior similar to that of the WT channel, with transitions among three conductance states. Its amplitude histogram, however, always showed only two recognizable peaks (∼70–75 and ∼25–30 pS), perhaps because the lowest-conductance state was so infrequently and briefly occupied at pH 7.6. The third column shows average amplitude histograms calculated from all of the individual histograms assigned to each category (pure mutant, A, B, C, D, or WT). The shapes of the group average histograms were similar to those of the individual examples, underscoring the uniqueness of the hybrid channel types. The broader peaks seen in the group average Type B and WT histograms reflect the variation we observed in the absolute amplitude (although not in the shape) of these channel types. Fig. 2 B shows the number of each channel type found, out of a total of 65 single-channel patches pulled from WT and E333G coinjected oocytes. As expected, the least common species were the homomultimeric WT channels (two observed) and pure mutant channels (six observed). Of the hybrid channels, Types A and B were found more than twice as frequently as Types C and D.

Fig. 3 shows amplitude histograms compiled from examples of the four hybrid channel types at a range of

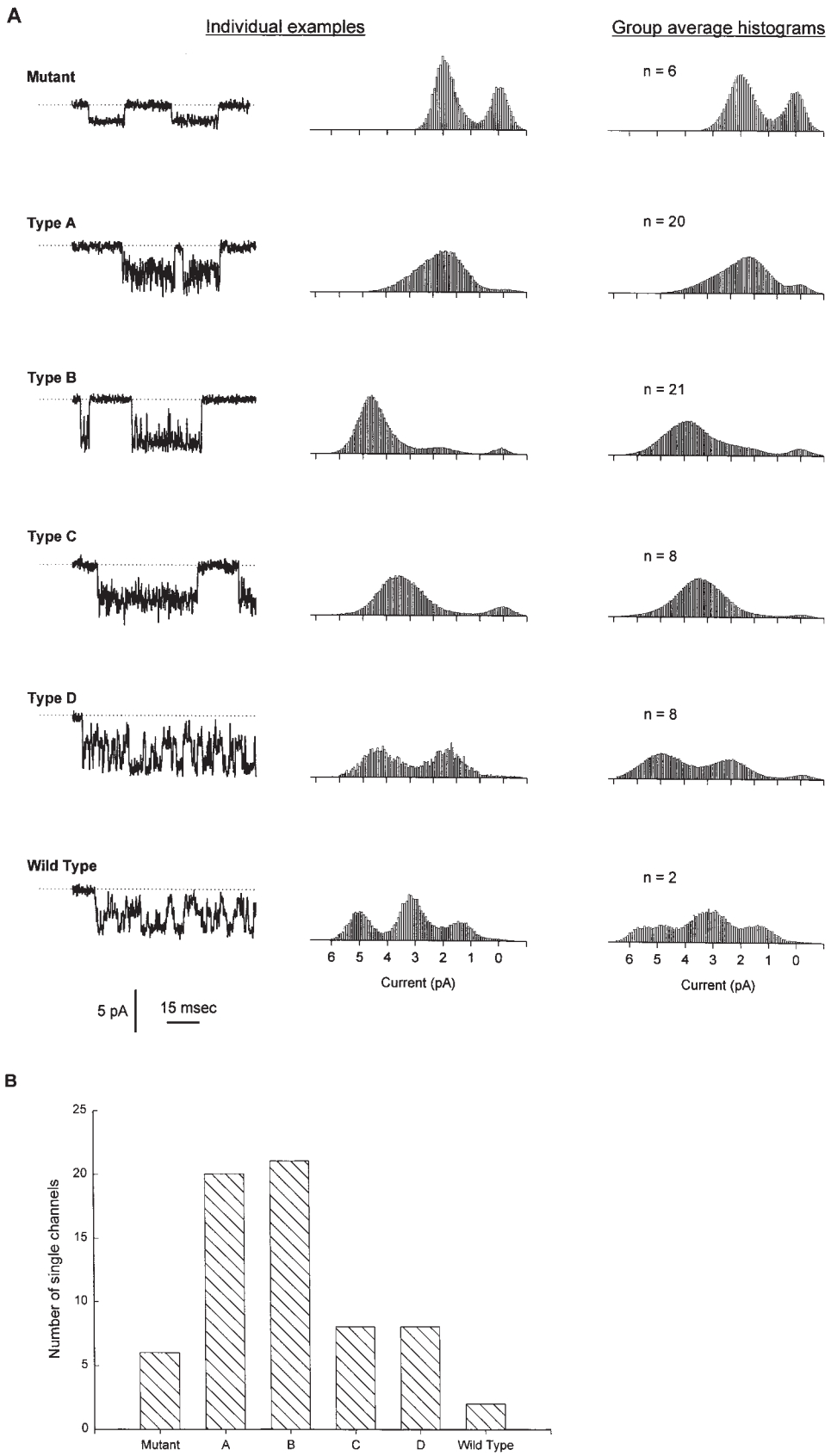

Figure 2. Injection of a mixture of WT and E333G CNG subunits gives rise to six types of channel behavior. (A) In addition to WT behavior (showing three distinct nonzero conductance states of 65–70, 35–40, and 15–20 pS; bottom) and pure mutant behavior (showing one nonzero conductance state of ∼25 pS; top), four hybrid types of CNG channel behavior were recorded and named Types A, B, C, and D. (Left and middle) For each channel type, a single-channel current record obtained at a holding potential of −80 mV with 130 mM NaCl, pH 7.6, on both sides of the membrane is shown alongside a corresponding amplitude histogram. Type A channels had noisy openings and gave an amplitude histogram with a low-conductance (∼31 pS) peak and a long high-conductance tail. Type B channels showed two distinct conductance states of ∼50–65 and ∼25–40 pS. Type C channels fluctuated widely about a conductance level of ∼55 pS, giving an amplitude histogram with one broad peak and tails extending to both low and high conductances. The single-channel behavior of Type D channels looked similar to WT behavior, although the Type D amplitude histogram calculated from many openings had two broad peaks (∼70–75 and ∼25–30 pS) rather than the three sharper peaks typical of WT channels. (Right) Average amplitude histograms calculated from all the histograms assigned to each category (pure mutant, A, B, C, D, and WT). For each hybrid channel, the group average histogram is similar to the individual example shown in the middle column, suggesting that the behavior of each of the hybrid channel types was unique. (B) Of 65 single channels recorded in patches from oocytes injected with a 2:1 mixture of WT and E333G CNG subunits, 6 mutant, 2 WT, and 57 hybrid channels were observed. Of the hybrid channels, Type A (n = 20) and Type B (n = 21) channels were found roughly twice as frequently as Types C and D channels (n = 8 for both).

extracellular pH values. Recordings were made from outside-out patches, and pH changes were made by moving the patches between microcapillary perfusion tubes. While the behavior of Type A channels did not change significantly between pH 8.5 and 6.0 (aside from a slight flattening of the high-conductance tail of the amplitude histogram), the behavior of Types B, C, and D was strongly pH dependent. Type B channels appeared to undergo a smooth transition from a well-defined high-conductance state to a well-defined low-conductance state as the pH was lowered. Type C channels also shifted to lower conductances at lower pH values, although it was not possible to discern two clearly separable conductance states. For the Type D channel, a transition between two well-defined conductance states at high pH was followed by a more gradual shift to lower conductances at low pH. While the amplitude distributions of Type B channels kept their distinctive two-peaked shape even at pH 6.0, the Type A, C, and D distributions all seemed to converge at low pH on a common shape having a low-conductance hump with a long, high-conductance tail.

The pH Dependence of the "Type B" Hybrid CNG Channel Is Consistent with Protonation at a Single Site

Of the four hybrid channels, the Type B channel, exhibiting two distinct conductance states over a wide pH range, seemed like the best candidate for a hybrid having one of the WT protonation sites. Amplitude histograms were compiled from Type B channel activity in outside-out patches at various values of extracellular pH and fitted to a sum of three Gaussian functions corresponding to the closed state and two open states of

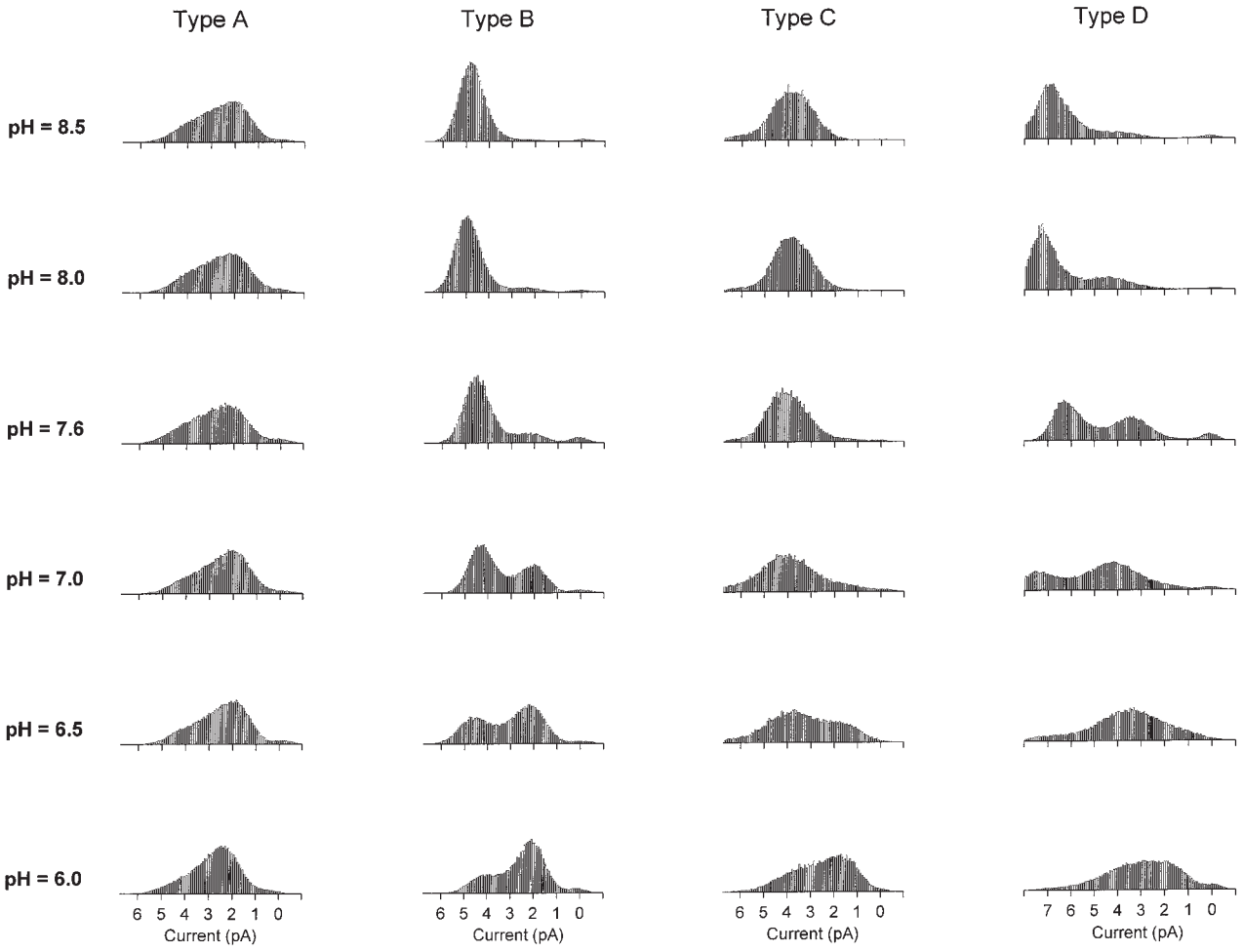

Figure 3. pH dependence of the hybrid CNG channels formed by coexpression of WT and E333G subunits. Amplitude histograms were compiled from single-channel currents recorded from outside-out patches with 130 mM NaCl on both sides of the membrane. Holding potential: −80 mV. The extracellular pH was varied by means of an array of capillary tubes (see materials and methods). For each channel type, all of the histograms in the figure were compiled from the same channel. Type A channels showed only a slight dependence on extracellular pH, while Types B, C, and D channels were strongly pH dependent. In particular, the Type B channel had two distinct conductance states at all pH values tested and switched smoothly from the high-conductance (∼50–65 pS) to the low-conductance (∼25–40 pS) state as the pH was lowered.

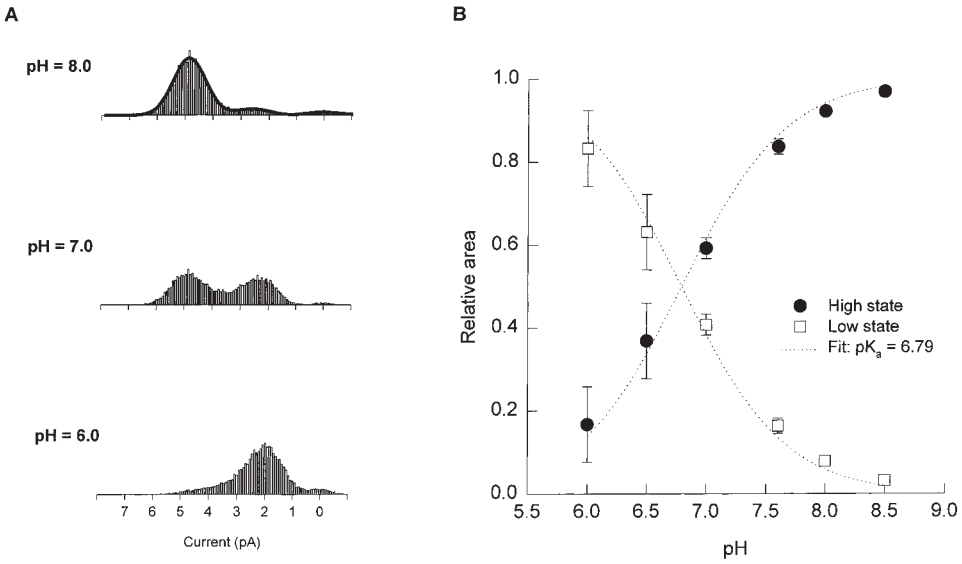

Figure 4. The pH dependence of the Type B hybrid CNG channel is consistent with there being a single protonation site. (A) Type B amplitude histograms (obtained from single-channel outside-out patches at a holding potential of −80 mV with 130 mM NaCl on both sides of the membrane) were compiled at different values of extracellular pH and fitted to a sum of three Gaussian functions, corresponding to the high and low conductance states and the closed state. Amplitude histograms collected from the same channel at pH_o 8.0, 7.0, and 6.0 are shown along with the three-Gaussian fit at pH_o 8.0 (solid line). The relative area under the low- and high-state Gaussian peaks was used as a measure of the probability of occupancy of each state as a function of pH_o. The intracellular pH was 7.6. (B) The relative area under the Gaussian functions corresponding to the high and low conductance states was plotted as a function of pH, along with a fit to a model in which the probability of occupying the low conductance state depends on protonation at a single site (dotted lines). In the model, $P_{\text{low state}} = 1/[1 + 10^{-(pKa - pH)}]$, where $pK_a = -\log[K_a]$ describes the binding affinity of the protonation site, and $P_{\text{high state}} = 1 - P_{\text{low state}}$. The fit gives a pK_a for the protonation site of 6.79.

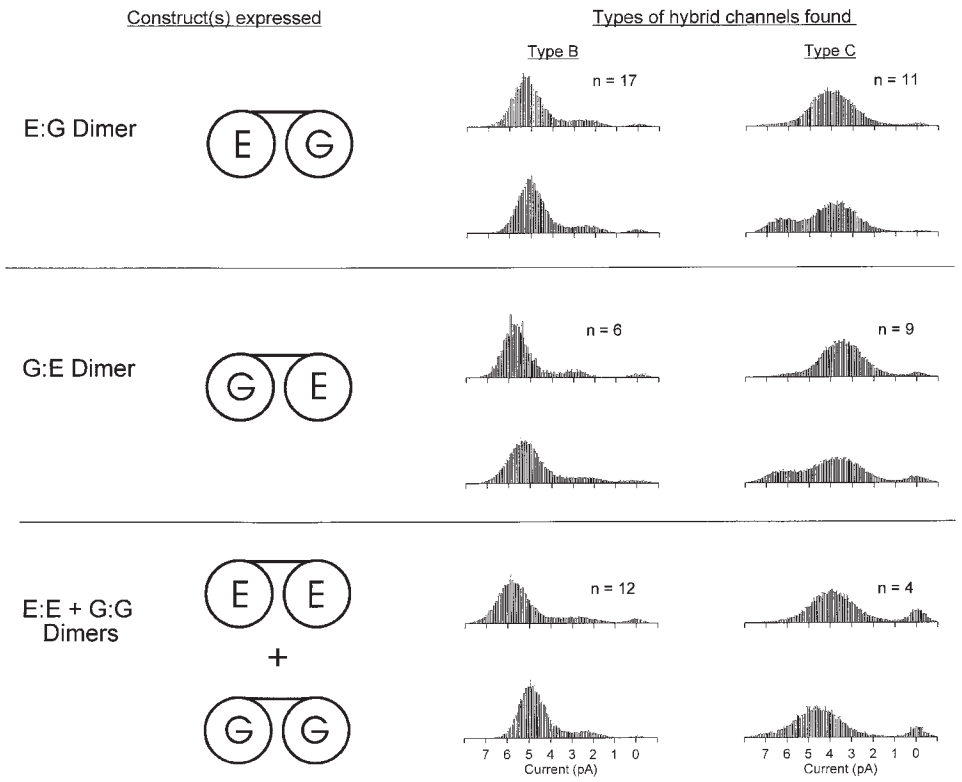

Figure 5. Expression of dimers of CNG subunits. Expression of the WT:E333G (E:G) dimer, the G:E dimer, or a 2:1 mixture of the E:E and G:G dimers gave rise to Types B and C hybrid channels, but never Types A or D channels. Two examples of each hybrid channel type seen are given along with the total number of each type observed. The examples were chosen to show the variations in single-channel behavior that we observed for each channel type: Type B channels had variable absolute single-channel amplitude (e.g., bottom left), and Type C channels rarely showed a small secondary peak in the amplitude histogram at high conductances rather than a smooth tail (seen in 2/11 Type C channels when the E:G dimer was expressed and 1/9 Type C channels when the G:E dimer was expressed; examples are shown in the top and middle rows, right). Amplitude histograms were computed from single-channel currents recorded in inside-out patches at a holding potential of −80 mV. The intra- and extracellular solutions both contained 130 mM NaCl, pH 7.6.

the channel. Fig. 4 A shows amplitude histograms from the same channel at three pH values; the top (pH 8.0) histogram appears with its three-Gaussian fit (solid line). The relative area under the Gaussian functions for the nonzero conductance states, a measure of the relative occupancy of the states, was calculated for three channels and plotted as a function of pH (Fig. 4 B). The dotted lines in Fig. 4 B show the predictions of a model in which transitions from the high to the low state are governed by protonation at a single site (see Fig. 4, legend). The good agreement with the data indicates that the steepness of the transition between states in the Type B channel is consistent with a single-site mechanism. The best fit to the data gives a pK_a for the single site of 6.8.

The Types B and C Hybrid Channels Contain Two WT and Two E333G Subunits

To gain a better understanding of the subunit composition of the hybrid CNG channels, we constructed and expressed tandem dimers of WT and E333G subunits. Our hypothesis was that the subunit composition of channels formed from dimers, instead of coexpressed monomers, would be more tightly constrained. In the optimal case, in which dimers associate in one orientation to form full tetrameric channels, one would expect expression of each single type of dimer to give rise to a single type of channel. The dimers used in these experiments consisted of two complete CNG subunits joined by a 34 amino acid linker (see materials and methods).

Fig. 5 shows the behavior of channels observed in inside-out patches after several types of dimers were expressed. Expression of the dimer consisting of a WT subunit linked in tandem to an E333G subunit (the E:G dimer, named after the residues at position 333 in each subunit) gave rise to two and only two of the hybrid channel types, Types B and C. These were identified on the basis of the shapes of their amplitude histograms at pH 7.6 and their pH dependence in outside-out patches (data not shown). Expression of the opposite dimer, G:E, gave the same two types of hybrid channels, as did expression of a 2:1 mixture of the E:E and G:G dimers (which also gave WT and pure mutant channels, not shown). The fact that expression of the E:G or G:E dimer alone produced more than one type of channel—as well as the fact that coexpression of the E:E and G:G dimers produced two different hybrid channels—suggested that the dimers were associating in more than one way.

One explanation for the data of Fig. 5 is that the CNG dimers can assemble into tetrameric channels in all three possible dimer–dimer configurations, illustrated in Fig. 6, top. In the first configuration (i), dimers associate "head-to-tail," with the A protomer of one dimer contacting the B protomer of the other. In

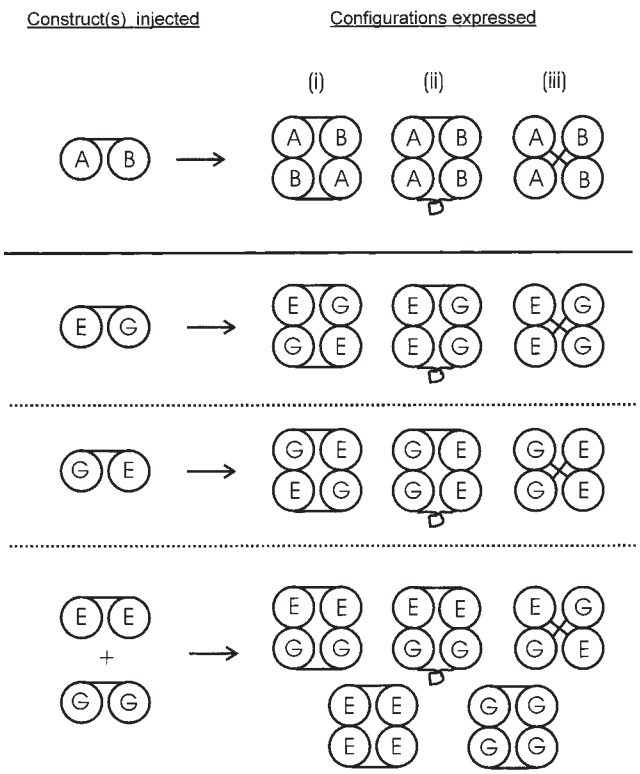

Figure 6. The results of expressing CNG channel dimers can be explained if the dimers can form tetrameric channels in three ways (top): (i) symmetrically, with the A and B protomers of the dimers across the channel from each other; (ii) asymmetrically, with the A and B protomers adjacent to each other; or (iii) with the two protomers of each dimer across the channel from one another. This scheme predicts that two (and only two) hybrid species should be formed when the E:G dimer, the G:E dimer, or a mixture of the E:E and G:G dimers are expressed, as observed experimentally. The two hybrid species, Types B and C, are each predicted to contain exactly two WT and two E333G subunits, with the WT subunits oriented across the channel from each other in one case and adjacent to each other in the other.

the second configuration (ii), dimers associate "head-to-head," with the A and B protomers of the two dimers contacting each other. In the third configuration (iii), the dimers interlock to form channels, and the A and B protomers of each dimer sit at opposite corners of the channel. This scheme depends on the assumptions that CNG channels are fourfold symmetric tetramers and that all of the dimers associate as dimers, contributing both of their subunits to each of the channel species formed.

As shown in Fig. 6, bottom, the first two configurations (i and ii) are sufficient to give two channel structures when the E:G or G:E dimer is expressed alone. These structures are each predicted to have two WT and two E333G subunits, with the WT subunits lying across the channel from each other (i) or adjacent to each other along a side of the channel (ii). When the E:E and G:G dimers are coexpressed, association in the

first two configurations would give rise to only one of these two structures (the structure having adjacent WT subunits), and it becomes necessary to invoke the third configuration (iii) to produce the structure having WT subunits at opposite corners of the channel. As indicated in the figure, coinjection of the E:E and G:G dimers would also be expected to give rise to WT and pure mutant channels.

If the scheme shown in Fig. 6 is correct, then the Type B and Type C channels each have two WT and two E333G subunits, with one of them having adjacent and the other opposite WT subunits; the data in Fig. 5 do not indicate with certainty which channel type corresponds to which arrangement. Regardless of their orientation, however, the presence of exactly two WT subunits, and hence two pore glutamates, in the Type B channel is a further indication that this channel could contain a single carboxyl-carboxylate that is similar to those formed in the pore of the WT channel.

Identities of the Type A and Type D Channels

Fig. 7 shows the types of channels observed in inside-out patches when the E:G dimer was coexpressed with either the G:G (top) or the E:E (bottom) dimer. In both cases, coexpression gave rise to the channels expected from expression of the dimers individually: pure mutant, Type B, and Type C channels for the coexpression of the E:G and G:G dimers; WT, Type B, and Type C channels for the coexpression of the E:G and E:E dimers (the pure mutant and WT channels are not shown in the figure). In both cases, an additional hybrid channel type was also found. For the E:G + G:G coexpression, this additional hybrid channel was the Type A channel, while for the E:G + E:E coexpression, the additional channel was the Type D channel. As before, the hybrid channels were identified based on the shapes of their amplitude histograms at pH 7.6 and their pH dependence in outside-out patches (not shown).

The additional hybrid channel produced in each case, not expected from expression of the dimers individually, most likely arose from the two coexpressed dimers coming together to form a unique channel. This implies that the Type A channel contained one WT subunit and three E333G subunits, while the Type D channel contained three WT subunits and one E333G subunit. Only one unique hybrid is expected in each case, since coassociation of the coexpressed dimers in all three of the configurations shown in Fig. 6, top, would give rise to the same subunit arrangement. Types A and D channels were never seen when the E:G, G:E, or E:E + G:G dimers were expressed (Fig. 5), consistent with the conclusion that they have a one WT, three mutant or three WT, one mutant subunit arrangement.

discussion

The Nature of the Protonation Sites in the Catfish Olfactory CNG Channel

The central goal of this study was to test the idea, proposed by Root and MacKinnon (1994), that the two

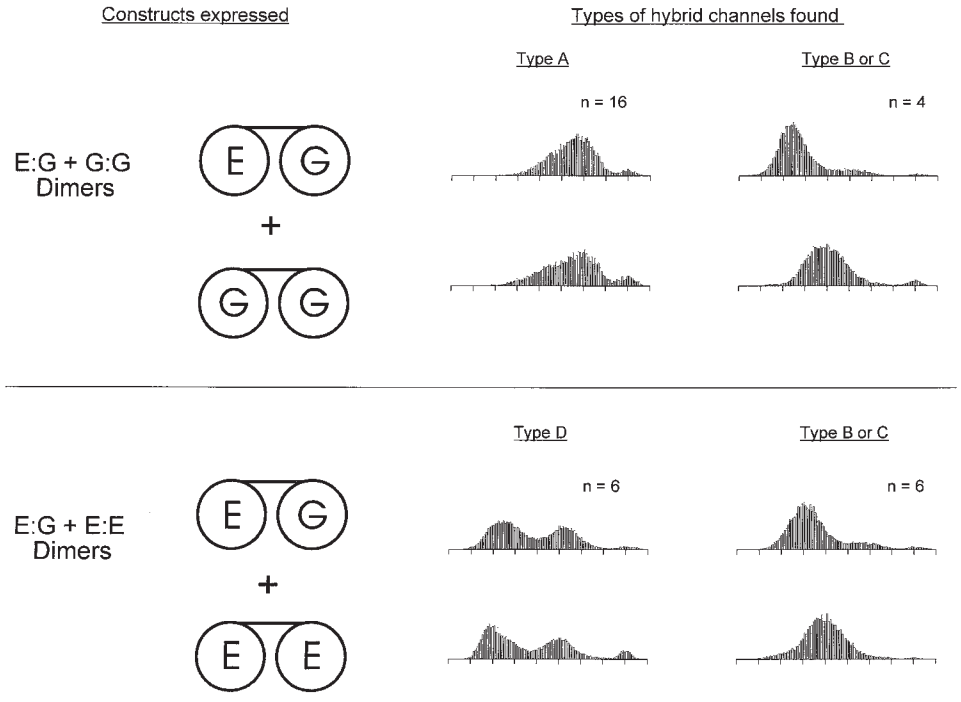

Figure 7. Expression of a mixture of the E:G and G:G dimers gave rise to Types A, B, and C, but never Type D, channels. Expression of a mixture of the E:G and E:E dimers gave rise to Types B, C, and D, but never Type A, channels. Examples of the measured hybrid channel types are given along with the total number of each type observed. Amplitude histograms were computed from single-channel currents recorded in inside-out patches at a holding potential of −80 mV. The intracellular and extracellular solutions contained 130 mM NaCl, pH 7.6.

proton-binding sites in the pore of the catfish olfactory CNG channel are physically independent carboxyl-carboxylate structures. In the WT channel, these sites are formed by four glutamate residues in the pore, one contributed by each of the channel subunits. Our strategy was to create hybrid channels containing varying numbers of pore glutamates and determine whether it was possible to isolate a hybrid species containing one, but not both, of the original protonation sites. By expressing a mixture of WT and E333G monomers and various combinations of dimers, we formed four easily distinguished hybrid types of CNG channels. One of the hybrid channels (Type B) had the properties expected of a channel containing a single proton acceptor site similar to the two in the WT channel: (a) it had two conductance states whose occupancy was controlled by protonation at a single site of pK_a 6.8, and (b) it contained two WT and two E333G subunits. Because our dimer constructs assembled into tetrameric channels in several ways, we were not able to determine whether the two glutamate residues in the Type B channel were positioned on adjacent or opposite subunits. Based on the equivalence and independence of the two sites in the WT channel (Root and MacKinnon, 1994), we might have expected that the Type B site would have a pK_a of exactly 7.6, not 6.8. This apparent inconsistency, however, is not very surprising. Independence of the two sites in the WT channel means that protonation of the one site is independent of protonation of the other site. However, that does not mean that protonation of one of the sites would be insensitive to complete removal of the glutamate side-chains comprising the other site. Side-chain removal is a much larger perturbation of the environment of the channel pore than addition of a proton. Therefore, these data strongly suggest that we were able to reconstitute individually in the Type B hybrid channel one of the carboxyl-carboxylate sites in the pore of the WT channel, which supports the notion that the sites in the WT channel are made from structurally independent glutamate pairs.

The present results, taken together with the earlier results of Root and MacKinnon (1994), suggest an arrangement of glutamates in the pore of the catfish olfactory CNG channel that is much different from the arrangement of the glutamates in the pore of the cardiac L-type Ca^{2+} channel. In the Ca^{2+} channel, the four pore glutamates are proposed to form an asymmetric cluster giving rise to a single protonation site, with each glutamate making a distinct contribution to the site and two of the glutamates, those in domains I and III of the channel, acting in concert to coordinate a proton (Chen et al., 1996; Chen and Tsien, 1997). In the catfish olfactory CNG channel, the four glutamates are apparently present in a symmetric ring such that they can form two identical pairs (upon the breaking of symmetry at the level of individual side chains). In light of these different arrangements, it is interesting to consider the different types of ion binding sites formed by the sets of glutamates in the two types of channels. The glutamates in the pore of the bovine retinal CNG channel form a high-affinity binding site for divalent cation blockers in the outer part of the channel pore (Root and MacKinnon, 1993), a role perhaps suited to their arrangement as a symmetrical ring of negative charge at a fixed position in the channel mouth. In contrast, the glutamates in the L-type Ca^{2+} channel form the essential sites for permeant Ca^{2+} ions in the pore, and therefore must, in accordance with the prevailing models of Ca^{2+} channel permeation, be able to accommodate two Ca^{2+} ions at a time—a function aided by the fact that they presumably constitute an asymmetrical glutamate cluster with mobile carboxylate moieties positioned at a range of depths in the tightest part of the pore (Kuo and Hess, 1993; Yang et al., 1993; Ellinor et al., 1995; Chen et al., 1996; Chen and Tsien, 1997).

Subunit Stoichiometry of the Catfish Olfactory CNG Channel

Given the homology between the channel under study and potassium channels, which have been shown to have a stoichiometry of four subunits per channel (MacKinnon, 1991; Liman et al., 1992; Doyle et al., 1998), it is tempting to postulate a tetrameric structure for the catfish olfactory CNG channel. The present results lend credence to this idea. Expressing a mixture of WT and E333G subunits gave WT channels, pure mutant channels, and four varieties of hybrid channels having easily distinguished, qualitatively different properties. Assuming that subunits contribute symmetrically to the channel, and assuming that the order of the glutamates around the channel pore is important, this number of hybrid channels is most simply explained if four subunits come together to form a complete channel. A symmetric three-subunit channel would be expected to give just two different hybrid structures, while a symmetric five-subunit channel would be expected to give six hybrid structures. Of course, the present results could arise from a channel structure with five or more subunits if some of the hybrid structures are degenerate, having different configurations of WT and E333G subunits but identical behavior as a function of pH, but a tetrameric channel provides the simplest explanation.

Our conclusion closely parallels the findings of Liu et al. (1996), who coexpressed the 30-pS WT bovine retinal CNG channel and an 85-pS chimeric bovine retinal channel containing the catfish olfactory CNG channel P region and counted the number of hybrid CNG channels, identified by their different conductances, that were produced. The authors observed four different in-

termediate conductance levels and concluded both that the channels formed were tetrameric and that the order of subunits around the channel pore was important. When these authors expressed dimer constructs, they found that association of the dimers primarily occurred in one configuration, the head-to-tail configuration shown in Fig. 6, (i), whereas our dimers appeared to associate in three different ways. The simpler behavior observed by Liu et al. (1996) could reflect the fact that the dimers used in those experiments did not include an extra peptide between the COOH terminus of the A protomer and the NH_2 terminus of the B protomer, or could reflect inherent differences in the association properties of retinal versus olfactory CNG channel subunits. The idea that bovine retinal CNG channel dimers might constrain subunit order better than catfish olfactory CNG channel dimers is also suggested by the experiments of Gordon and Zagotta (1995) exploring the intersubunit coordination of Ni^{2+} ions by retinal CNG channels. The authors found quantitative evidence that subunit order was well constrained in these experiments, even though a 21 amino acid linker was used between retinal CNG subunits (comparable with the 34 amino acid linker used in our experiments).

Molecular Identities of the Hybrid CNG Channels

Expression of CNG channel dimers made it possible to draw conclusions about the subunit makeup of the four types of hybrid channels we observed when WT and E333G monomers were coexpressed. Fig. 8 shows the possible WT and E333G subunit combinations expected for a tetrameric channel and correlates these combinations with the hybrid channels that were observed. The Type A channel could be unambiguously assigned to a specific structure since coexpression of the E:G + G:G dimer combination was not sensitive to the variability of dimer association. Since the Type A channel arose uniquely when the E:G and G:G dimers were coexpressed, we conclude that this channel has only one WT subunit and therefore only one pore glutamate. This is consistent with this channel's lack of a strong pH dependence between pH 8.5 and 6.0, since one would expect a lone carboxyl group to have a pK_a several units lower.

The Type B and Type C channels each contain two WT and two E333G subunits, although the flexibility of dimer association prevented us from determining which of these had two adjacent WT subunits and which had two opposite WT subunits. This leaves doubt as to the precise configuration of the carboxyl-carboxylate interaction in the Type B channel—it is possible that it occurs across the channel between opposite subunits or along a side of the channel between adjacent subunits. Which of these possibilities is more plausible depends critically on the position and angle at which

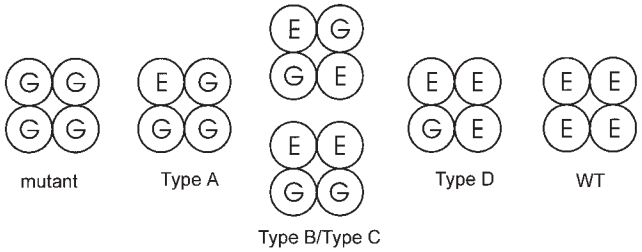

Figure 8. Identities of the six types of channels observed after expression of a mixture of WT and E333G CNG subunits, as deduced through dimer expression. Hybrid channel Types A and D can be assigned to specific structures: Type A has one WT subunit and three Glu333Gly subunits, while Type D has three WT subunits and one Glu333Gly subunit. Types B and C each have two WT and two E333G subunits, although it cannot be determined which channel type has two adjacent WT subunits (Type B/Type C, bottom) and which has two WT subunits opposite one another (Type B/Type C, top).

Glu333 projects into the channel pore. The fact that the Type C channel does show pH dependence between pH 8.5 and 6 presents the possibility that its two glutamates can combine to form a protonation site of fairly high pK_a. Fig. 3 suggests that in this channel, protonation at a site with a pK_a of $\sim$6.25 causes a gradual shift to a lower conductance state of $\sim$20–25 pS. The Type C channel resembles the EIIQ L-type Ca^{2+} channel mutation studied by Chen et al. (1996) in two respects: (a) it flickers from its main conductance level to higher and lower conductance levels (as shown in Fig. 2 A); and (b) as the pH is lowered, the lower conductance state becomes populated, but the flickers between the middle- and high-conductance states remain, suggesting that the distribution between the high and middle states does not change with increasing $[H^+]$. This analogous behavior is intriguing, especially considering that the Type C channel is expected to contain a twofold symmetric arrangement of two glutamates, while the EIIQ Ca^{2+} channel is expected to contain an asymmetric arrangement of three glutamates. It will be interesting to compare further the structure and ion conduction properties of these two channels in search of a common mechanism underlying their similar single-channel behavior.

The Type D channel, which arose uniquely when the E:G and E:E dimers were coexpressed, could be unambiguously assigned to a structure having three WT subunits (and hence three pore glutamates). Consequently, its conductance shows strong pH dependence. Since this channel has glutamates positioned next to each other and across the channel from each other, it should accept protons both like a Type B and like a Type C channel. This is consistent with the pH dependence shown in Fig. 3, which shows a clear Type B–like transition between two conductance states at high pH

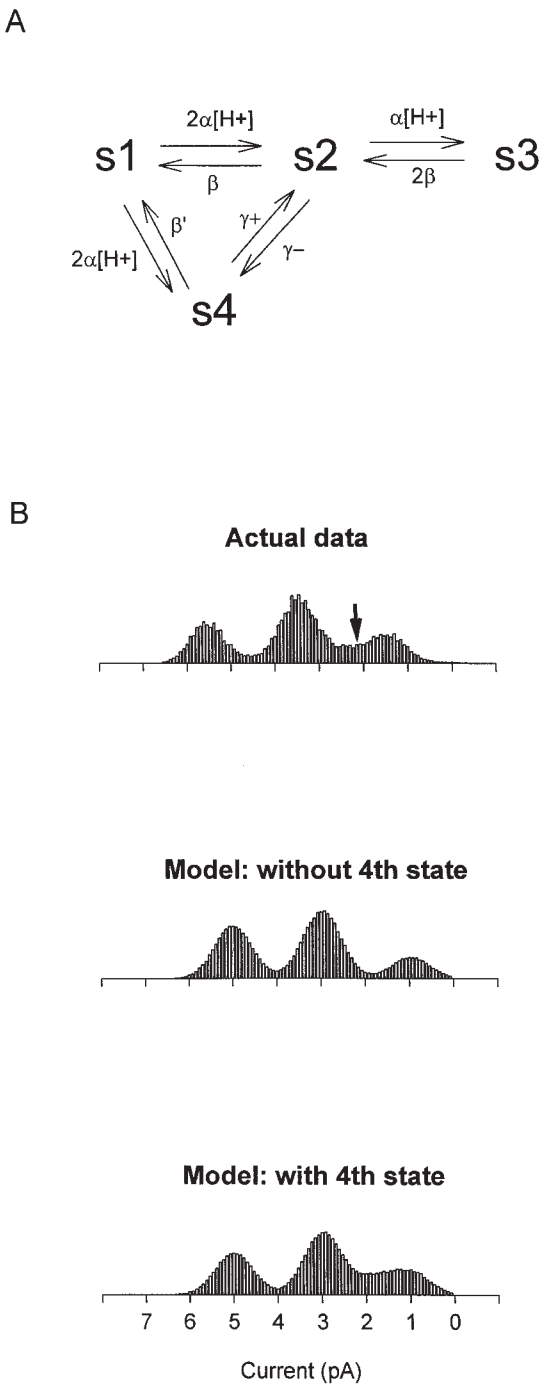

Figure 9. Model of WT channel behavior including both Type B and Type C modes of protonation. (A) The model includes four conductance states, s1–s4. s1 is the highest conductance state (65–70 pS) and occurs when no proton is bound to the channel pore. s2 (40–45 pS) occurs when one of the independent and equivalent carboxyl-carboxylate sites is occupied by a proton, and s3 (15–20 pS) occurs when both carboxyl-carboxylate sites are occupied. s4 (∼20–25 pS) occurs when a proton binds to the pore in the alternate, Type C, mode. The rate of proton binding is assumed to be diffusion limited for both modes of protonation. The pK_a for the Type B carboxyl-carboxylate sites is taken to be 7.6, while the pK_a for the Type C site is estimated to be ∼6.25. Concerted transitions can occur between s4 and s2 and are represented by the rate constants γ^+ and γ^-. Model parameters (explained more fully in the text): $\alpha = 6.4 \times 10^9\ M^{-1}*s^{-1}$, $\beta = 200\ s^{-1}$, $\beta' = 1{,}920\ s^{-1}$, $\gamma^+ = 1{,}920\ s^{-1}$, and $\gamma^- = 200\ s^{-1}$. Gaussian noise was added to the modeled channel transitions to construct realistic amplitude histograms. The model simulations were performed using a Microsoft QuickBASIC program implemented on a personal computer. (B) Comparison of model simulations with WT channel data. (Top) Amplitude histogram calculated from the activity of a single WT channel recorded at pH 7.6 with 130 mM NaCl on both sides of the membrane (the holding voltage was −80 mV). WT channels visited current levels between the low- and middle-conductance states more often than expected, giving rise to extra density in this part of the amplitude histogram (arrow). (Middle) Amplitude histogram generated from the model with s4 omitted. (Bottom) Histogram generated from the model with s4 included. Inclusion of s4 can reproduce the extra density seen in WT amplitude histograms, suggesting that a second mode of protonation is needed to fully explain WT channel behavior.

followed by a less well-resolved Type C–like transition to a lower conductance state at lower pH.

The WT channel, containing all four glutamates, would also be expected to show both Type B and Type C behavior. Protonation in the Type B mode (i.e., via independent carboxyl-carboxylate interactions) would give the transitions among three clear conductance states that are the hallmark of this channel. Protonation in the Type C mode, causing a poorly resolved transition to an intermediate conductance state, might be expected to affect the behavior of the WT channel more subtly.

We modeled this effect by adding a fourth conductance state to the channel, as depicted in Fig. 9 A. In the model, Type B protonation at the two independent and equivalent carboxyl-carboxylates causes transitions along the top row of states, from the high-conductance state s1 (65–70 pS) to the middle- and low-conductance states, s2 (40–45 pS) and s3 (15–20 pS) (these are the same transitions diagrammed in Fig. 1 C). Type C protonation shifts the channel to an intermediate state s4 whose conductance, estimating from Fig. 3, is ∼20–25 pS, between the conductances of s2 and s3, an estimate that depends on the assumption that protonation in the Type C mode has the same effect on the WT channel, which has four pore glutamates, as on the Type C channel, which has only two glutamates. In theory, a second Type C protonation is possible in the WT channel, which would be expected to give rise to a fifth conductance state in which both Type C sites are occupied. However, since we could only measure one Type C transition in the Type C channel (which contains only two glutamates), and since we have no way of predicting the pH range of the second Type C protonation or its effect on the channel conductance, we limit our model to only one Type C transition. This model is therefore incomplete and should be regarded as a first approximation.

Because Type C, like Type B, protonation should occur in the WT channel at either of two sites and is assumed to be diffusion limited, we take the transition rate from s1 to s2 or s4 to equal $2\alpha[H^+]$, where $\alpha = 6.4 \times 10^9\ M^{-1}{*}s^{-1}$ (following Root and MacKinnon, 1994). While β, the proton off rate from the carboxyl-carboxylates, must be set at 200 s^{-1} to give a pK_a of 7.6 for these sites, β', the off rate of protons from the Type C site, must be adjusted to 1,920 s^{-1} to account for the lower pK_a of the Type C site, estimated from Fig. 3 to be ~6.25. The model allows concerted transitions between s2, in which a single proton is bound in the Type B configuration, and s4, in which it is bound in the Type C configuration. The rates of such transitions are assumed to be of the same order of magnitude as the rates of exit from s2 and s4 to s1; this, along with the assumption of microscopic reversibility around the s1–s2–s4 loop, sets γ^+ at 1,920 s^{-1} and γ^- at 200 s^{-1}.

Fig. 9 B compares a WT amplitude histogram recorded at pH 7.6 and −80 mV with amplitude histograms generated from the model under the same conditions and suggests that Type C protonation in the WT channel might explain a subtle but consistent feature of WT behavior. As indicated by the arrow in Fig. 9 B, the WT channel consistently tends to visit current levels between the low- and middle-conductance states more often than expected; the extra density in this region is greater than can be explained by overlap of the Gaussian functions for the two neighboring states. This feature was observed in every WT channel recorded in this study (see Figs. 1 and 2) and is evident in the original data of Root and MacKinnon (1994). Fig. 9 B shows how inclusion of the second type of protonation, which allows the channel to make brief transitions to s4, can explain this extra density between 20 and 30 pS (~1.5–2.5 pA at −80 mV). Simulations of the WT channel including s4 were also better than simulations without s4 in predicting the behavior of the WT channel at other pH values (not shown). Thus, protonation at the two equivalent and independent Type B sites, while necessary to explain transitions among the three major conductance states, is not sufficient to explain WT channel behavior in its full detail. To capture all of the nuances of the channel's behavior, we must invoke a second, lower-affinity type of configuration in which the pore glutamates can pair to accept protons.

We thank Michael J. Root and Chul-Seung Park for helpful discussions.

This work was supported by National Institutes of Health grant GM47400 and by a Harvard Medical School Department of Neurobiology Quan Predoctoral Fellowship (to J.A. Morrill). R. MacKinnon is an Investigator in the Howard Hughes Medical Institute.

Submitted: 15 March 1999 Revised: 18 May 1999 Accepted: 19 May 1999

references

Chahine, M., A.L. George, M. Zhou, S. Ji, W. Sun, R.L. Barchi, and R. Horn. 1994. Sodium channel mutations in *Paramyotonia congenita* uncouple inactivation from activation. *Neuron*. 12: 281–294.

Chen, X.-H., I. Bezprozvanny, and R.W. Tsien. 1996. Molecular basis of proton block of L-type Ca^{2+} channels. *J. Gen. Physiol.* 108: 363–374.

Chen, X.-H., and R.W. Tsien. 1997. Aspartate substitutions establish the concerted action of P-region glutamates in repeats I and III in forming the protonation site of L-type Ca^{2+} channels. *J. Biol. Chem*. 272:30002–30008.

Cuello, L.G., J.G. Romero, D.M. Cortes, and E. Perozo. 1998. pH-dependent gating in the *Streptomyces lividans* K^+ channel. *Biochemistry.* 37:3229–3236.

Davies, N.W., N.B. Standen, and P.R. Stanfield. 1992. The effect of intracellular pH on ATP-dependent potassium channels of frog skeletal muscle. *J. Physiol.* 445:549–568.

Doyle, D.A., J.M. Cabral, R.A. Pfuetzner, A. Kuo, J.M. Gulbis, S.L. Cohen, B.T. Chait, and R. MacKinnon. 1998. The structure of the potassium channel: molecular basis of K^+ conduction and selectivity. *Science.* 280:69–77.

Ellinor, P.T., J. Yang, W.A. Sather, J.-F. Zhang, and R.W. Tsien. 1995. Ca^{2+} channel selectivity at a single locus for high-affinity Ca^{2+} interactions. *Neuron*. 15:1121–1132.

Gordon, S.E., and W.N. Zagotta. 1995. Subunit interactions in coordination of Ni^{2+} in cyclic nucleotide–gated channels. *Proc. Natl. Acad. Sci. USA*. 92:10222–10226.

Gordon, S.E., J.C. Oakley, M.D. Varnum, and W.N. Zagotta. 1996. Altered ligand specificity by protonation in the ligand binding domain of cyclic nucleotide–gated channels. *Biochemistry.* 35: 3994–4001.

Goulding, E.H., J. Ngai, R.H. Kramer, S. Colicos, R. Axel, S.A. Siegelbaum, and A. Chess. 1992. Molecular cloning and single-channel properties of the cyclic nucleotide–gated channel from catfish olfactory neurons. *Neuron*. 8:45–58.

Klockner, U., and G. Isenberg. 1994. Calcium channel current of vascular smooth muscle cells: extracellular protons modulate gating and single channel conductance. *J. Gen. Physiol.* 103:665–678.

Krafte, D.S., and R.S. Kass. 1988. Hydrogen ion modulation of Ca^{2+} channel current in cardiac ventricular cells. Evidence of multiple mechanisms. *J. Gen. Physiol.* 91:641–657.

Kuo, C.C., and P. Hess. 1993. Characterization of the high-affinity Ca^{2+} binding sites in the L-type calcium channel pore in rat phaeochromocytoma cells. *J. Physiol.* 466:657–682.

Liman, E.R., J. Tytgat, and P. Hess. 1992. Subunit stoichiometry of a mammalian K^+ channel determined by construction of multimeric cDNAs. *Neuron*. 9:861–871.

Liu, D.T., G.R. Tibbs, and S.A. Siegelbaum. 1996. Subunit stoichi-

ometry of cyclic nucleotide–gated channels and effects of subunit order on channel function. *Neuron*. 16:983–990.

MacKinnon, R. 1991. Determination of the subunit stoichiometry of a voltage-activated potassium channel. *Nature.* 350:232–235.

Prod'hom, B., D. Pietrobon, and P. Hess. 1987. Direct measurement of proton transfer rates to a group controlling the dihydropyridine-sensitive Ca^{2+} channel. *Nature.* 329:243–246.

Reyes, R., F. Duprat, F. Lesage, M. Fink, M. Salinas, N. Farman, and M. Lazdunski. 1998. Cloning and expression of a novel pH-sensitive two pore domain K^+ channel from human kidney. *J. Biol. Chem.* 273:30863–30869.

Root, M.J., and R. MacKinnon. 1993. Identification of an external divalent cation-binding site in the pore of a cGMP-activated channel. *Neuron*. 11:459–466.

Root, M.J., and R. MacKinnon. 1994. Two identical noninteracting sites in an ion channel revealed by proton transfer. *Science.* 265: 1852–1856.

Sawyer, L., and M.N. James. 1982. Carboxyl–carboxylate interactions in proteins. *Nature.* 295:79–80.

Traynelis, S.F., and S.G. Cull-Candy. 1991. Pharmacological properties and H^+ sensitivity of excitatory amino acid receptor channels in rat cerebellar granule neurones. *J. Physiol.* 433:727–763.

Yang, J., P.T. Ellinor, W.A. Sather, J.-F. Zhang, and R.W. Tsien. 1993. Molecular determinants of Ca^{2+} selectivity and ion permeation in L-type Ca^{2+} channels. *Nature.* 366:158–161.

Zhang, J.-F., and S.A. Siegelbaum. 1991. Effects of external protons on single cardiac sodium channels from guinea pig ventricular myocytes. *J. Gen. Physiol.* 98:1065–1083.